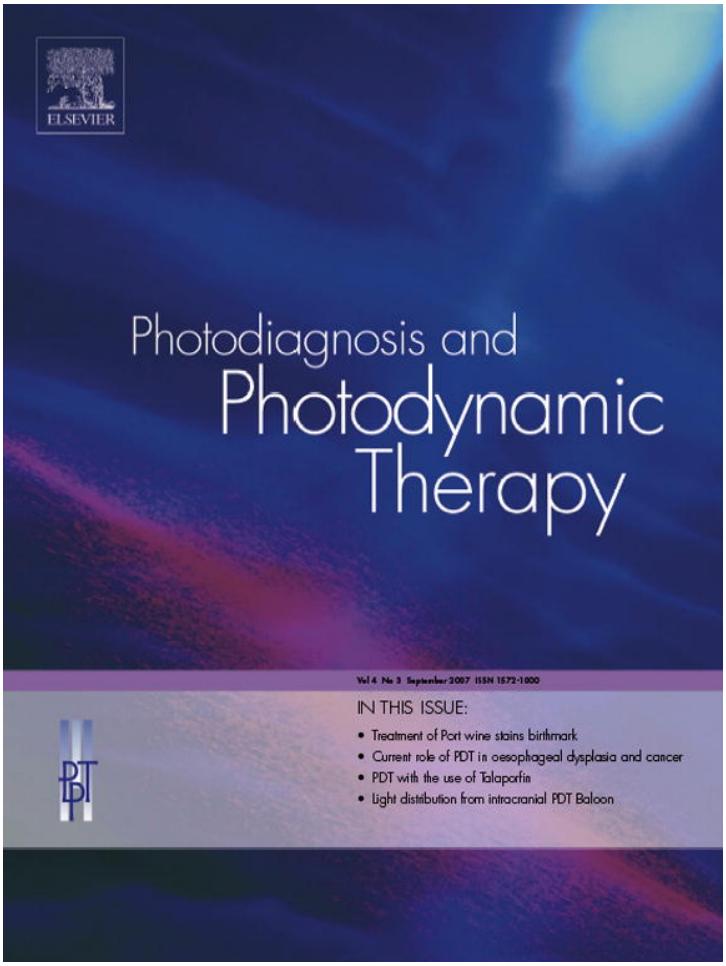

Photodiagnosis and Photodynamic Therapy (2007) 4, 190—196

available at www.sciencedirect.com

ScienceDirect

journal homepage: www.elsevier.com/locate/pdpdt

Visualization of basal cell carcinoma by fluorescence diagnosis and independent component analysis

Ivica Kopriva PhD[a,*], Antun Peršin[a], Hrvoje Zorc[a], Aida Pašić[b], Jasna Lipozenčić[b], Krešimir Kostović[b], Martin Lončarić[a]

[a] *Rudjer Bošković Institute, Bijenička cesta 54, 10002 Zagreb, Croatia*
[b] *Clinic of Dermatovenerology, Šalata 4, 10000 Zagreb, Croatia*
Available online 20 July 2007

KEYWORDS
Basal cell carcinoma;
Photodynamic detection;
Fluorescence imaging;
5-Aminolevulinic acid;
Independent component analysis

Summary Photodynamic detection (PDD) of skin tumours is based on the visualization of a fluorophores, with the ability to accumulate in tumour tissue, by the use of fluorescence imaging. Of particular importance is the application of δ-5-aminolaevulinic acid (ALA) that, through the process of biosynthesis causes formation of the protoporphyrin IX (PpIX). The PpIX has the ability of selective fluorescence after basal cell carcinoma (BCC) has been treated with ALA. Higher concentration of PpIX in tumour tissue compared to surrounding normal skin is the basis for PDD. Our contribution in this preliminary study is application of the independent component analysis (ICA) to extract the BCC spatial map, by processing fluorescent RGB image acquired under excitation with 405 nm light. Comparative performance analysis with other two widely used image processing methods: ratio imaging and optimal threshold based imaging, reveals that ICA produces BCC spatial map that is most consistent in term of diagnostic quality by both visual assessment and calculation of the BCC demarcation line. We believe this represents a solid basis for the design of a compact and low-cost multi-spectral fluorescence imaging system, capable for real time calculation of the skin tumour demarcation.

Introduction

Basal cell carcinoma (BCC) is steadily increasing year by year in most countries and accounts for about 80% of all non-melanoma skin cancers [1]. A non-invasive diagnostic technique for skin tumour demarcation, with the potential to move to clinical use, is therefore of great interest. Fluorescence imaging is such a technique; it is based on digital registration of the fluorescence obtained from fluorophores present in the tissue [1—6]. A photo sensitizer widely used in clinical applications is: 5-aminolevulinic acid (ALA) induced protoporphyrin IX (PpIX) [1—6]. ALA is a non-fluorescent precursor of fluorescent PpIX, with a degree of selective accumulation shown in a variety of malignancies [7]. Thus, by using low intensity excitation light, the PpIX can be located in the tissue by virtue of its fluorescence. Visualization of the PpIX represents the basis of the photodynamic detection (PDD) of the skin tumours and has been exploited in the design of the fluorescence imaging systems [1—6,8].

Fluorescence ratio imaging is a method widely used for the optical diagnosis of the BCC after administration of ALA induced PpIX [1,2,5]. It is based on calculating the ratio between red intensity (600—700 nm) over the blue/green intensity (450—550 nm). Owing to the fact that auto fluores-

* Corresponding author. Fax: +385 1 4680 104.
E-mail address: ikopriva@gmail.com (I. Kopriva).

1572-1000/$ — see front matter © 2007 Elsevier B.V. All rights reserved.
doi:10.1016/j.pdpdt.2007.03.004

cence intensity from normal tissue is higher in a tumour, in the range 450—550 nm, but lower in the range 600—700 nm, the contrast between tumour and adjacent normal tissue is enhanced significantly. Preliminary results reported in [1] confirmed good agreement with the histopathological extent of the tumour, implying that the technique can be applied as a useful tool for indicating tumour boundary of aggressive BCCs. This result will represent the basis for the later statement, regarding the quality of the BCC spatial maps, extracted by the independent component analysis (ICA) algorithm in a visual assessment of the demarcation of the BCC. It has been also reported in [1] that ratio imaging technique works well on plane skin surfaces, where it can be used as a preoperative screening tool but, is unsuitable on areas with extreme curvature, e.g. on the alar regions of the nose or, on external ear, where the technique is not reliable. This is due to the co-registration problem between the red and the blue/green intensity images. Another concern has been reported in [8] regarding the variation between different sets of images and absolute measurements of the fluorescence level. Because ratio-imaging methods are based on a division between the red intensity and green intensity, dynamic range of the ratio image is large. Therefore, additional post processing is necessary for the purpose of contrast enhancement. One way of doing it is to classify as a tumour every location of the ratio image that exceeds the predefined threshold value, which effectively produces the binary image of the tumour spatial map. The optimal threshold value however, depends on the intensity of the acquired fluorescence image. This is where the ratio imaging method can introduce errors in the estimation of the spatial tumour maps, as will be illustrated later in Fig. 6A and B.

An alternative to ratio imaging in the optical diagnosis of the BCC is threshold based imaging [4]. It classifies as BCC everything that is above cI_a, where I_a represents average intensity of the region with healthy skin, and c represents the factor that has been empirically found to be $c \approx 1.4$ for 3—4 h of ALA application.

To some extent, heuristic based threshold definition; together with the variation of absolute measurement levels of ratio imaging motivates consideration of an alternative method for the optical diagnosis of the BCC. ICA is a relatively novel theory derived for unsupervised analysis of the multivariate data sets [9,10]. Over the last 10 years it has found a numerous applications in a variety of scientific and engineering disciplines. Of the interest for the optical diagnosis of the BCC is the capability of the ICA algorithms for unsupervised segmentation of multi-spectral and hyper spectral images [11,12]. Unsupervised segmentation by ICA is based on the assumption of statistical independence between different classes resident in the multi-spectral image, where for example one class is a BCC and another class is a healthy surrounding skin tissue. Because statistical independence is a scale invariant feature, it is expected that ICA will be insensitive to the variation between the set of images of the absolute level of the measured fluorescence. Another principal reason for using ICA in optical diagnosis of the skin tumour is that it is applied on the co-registered band images and should not be sensitive on the type of problems that arise from the miss-registration.

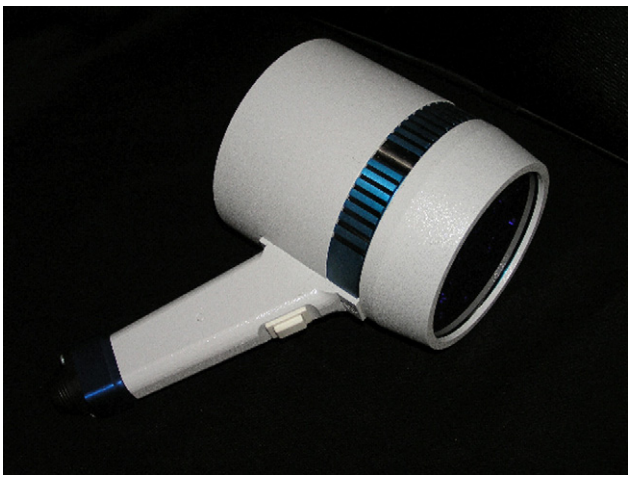

Figure 1 The apparatus developed for acquiring fluorescence image.

Materials and methods

Fluorescence imaging

Fig. 1 shows the apparatus developed for acquisition of the fluorescence image. It consists of 405 nm excitation light source and an RGB camera for the acquisition of the fluorescence image of the ALA treated BCC. The excitation light source has a spectral distribution centred at 405 nm, which matches the absorption spectrum of PpIX. The fluorescence emission spectrum of PpIX has a dominant peak at 635 nm. A base cream containing 20% of ALA was applied on the lesion and approximately 0.5 cm of the surrounding skin. The cream was applied for 4 h to obtain optimal PpIX contrast between tumour and normal skin [1,4]. After the 4 h period before imaging any residual ALA has been removed. The RGB image has been acquired in 1—2 s by a commercial digital camera. Although an RGB image is not a multi-spectral image in the true sense, it is suitable for the application of the multivariate data analysis methods such as, principal component analysis (PCA) and ICA in order to achieve unsupervised extraction of the BCC spatial map. This holds true as long as the image scene consists of three or less classes with a simple structure. By simple structure we assume that BCC and healthy skin are spectrally different in a coarse spectral resolution of an RGB image.

Multi-spectral imaging

Multi-spectral and hyper spectral imaging is a new research area that is already widely used in remote sensing [11—14] but also in fluorescence imaging [8] for object detection, classification and identification. A 3D image cube contains co-registered images for the same scene. In a number of real applications, in remote sensing image classification, it may be very difficult or even impossible to get prior information about class spectral signatures. Therefore, unsupervised methods have to be applied. Linear spectral un-mixing analysis is a popular approach used in decomposition problem. This procedure assumes the reflectance of a pixel is a linear mixture of all the different materials found in that pixel

[11–14]. Let L be the number of spectral bands and $\mathbf{r}$ a column pixel vector with dimension L in a multi-spectral image. An element r_i in the $\mathbf{r}$ is the reflectance collected in the ith wavelength band. Let $\mathbf{M}$ denote a matrix containing p independent material spectral signatures (referred to as end members in linear mixture model), i.e. $\mathbf{M} = [\mathbf{m}_1, \mathbf{m}_2, \ldots, \mathbf{m}_p]$. Let $\boldsymbol{\alpha}$ be the unknown abundance column vector of size $p \times 1$ associated with $\mathbf{M}$, which is to be estimated. The ith item α_i in $\boldsymbol{\alpha}$ represents the abundance fraction of $\mathbf{m}_i$ in pixel $\mathbf{r}$. In order to relate the linear mixture model Eq. (1) to the BCC localization problem we mention that the column vector $\mathbf{m}_i$ represents spectral signature of the BCC or healthy skin and $\{\alpha_i\}$ represent their respective spatial maps. Accordingly, the linear mixture model is:

$$\mathbf{r} = \mathbf{M}\boldsymbol{\alpha} + \mathbf{n} \tag{1}$$

where $\mathbf{n}$ is the noise term. When $\mathbf{M}$ is known the estimation of $\boldsymbol{\alpha}$ can be accomplished by a least squares approach. This is referred to as a supervised classification. In this case, it is assumed that spectral library with the stored spectral signatures $\mathbf{m}_i$ exists. But when $\mathbf{M}$ is also unknown, i.e., in unsupervised analysis, the task is much more challenging, because both $\mathbf{M}$ and $\boldsymbol{\alpha}$ need to be estimated.

Independent component analysis

ICA is a powerful tool for unsupervised classification, which has been successfully applied to blind source separation [9,10]. The basic idea is to decompose a set of multivariate signals into a basis of statistically independent sources, with the minimal loss of information content so as to achieve detection and classification. The standard linear ICA-based data model with additive noise is:

$$\mathbf{x} = \mathbf{A}\mathbf{s} + \mathbf{n} \tag{2}$$

where $\mathbf{x}$ is an L dimensional data vector, $\mathbf{A}$ an unknown mixing matrix, and $\mathbf{s}$ is an unknown source signal vector. Thus, the model (2) is structurally equivalent to the linear mixture model (1). Three assumptions are made on the unknown source signal vector $\mathbf{s}$: (1) each source signal is an independent identically distributed (i.i.d.) stationary random process; (2) the source signals are statistically independent at any time; and (3) at the most one among the source signals has Gaussian distribution. The mixing matrix $\mathbf{A}$, although unknown, is also assumed to be non-singular. Then the solution to the blind source separation problem, is obtained with the scale and permutation indeterminacy, i.e., $\mathbf{Q} = \mathbf{W}\mathbf{A} = \mathbf{P}\boldsymbol{\Lambda}$, where $\mathbf{W}$ represents the un-mixing matrix, $\mathbf{P}$ a generalized permutation matrix and $\boldsymbol{\Lambda}$ is a diagonal matrix. These requirements ensure the existence and uniqueness of the solution, to the blind source separation problem up to the ordering, sign and scale [9,10]. Thus, ICA algorithms possess the scale invariance property that makes them attractive for use in optical diagnosis of the BCC, from the RGB fluorescence image, with the absolute fluorescence level that may vary from measurement to measurement. For our purpose the following applies: $L = 3$ and $p = 1$. This implies that we are interested in the one class only: the BCC. Another class, the healthy tissue, is of no particular interest to us. Consequently, the sequential ICA algorithms are of special interest. They are capable of extracting the classes of interest in a sequential mode, i.e. one by one. The well-known fast ICA algorithm belongs to this class of algorithms [9,15]. In the extreme case it is desirable to be able to extract only one class of interest. In this particular case, in addition to statistical independence and non Gaussian distribution of data, there ought to be available some additional *a priori* information about the signal of interest. In the case of BCC this additional information is related to the fact that tumour, especially in the early phase of development, occupies relatively small portion of the overall area of the image. Such image after 2D to 1D mapping behaves as a random process, characterized by sparse distribution law. Thus, the measure for signal sparseness, that simultaneously measures the distance of signal distribution from the Gaussian or normal distribution, represents a good candidate for a cost function to be used in formulation of the algorithm for the BCC localization. Such measure is called *kurtosis* and for centred random variable $\mathbf{x}$ it is defined as the ratio of the fourth order moment and square of the second order moment:

$$\kappa(\mathbf{x}) = \frac{m_4(\mathbf{x})}{(m_2(\mathbf{x}))^2} - 3 \tag{3}$$

Assuming that tumour is a sparsest class contained in acquired fluorescent RGB image extraction of the BCC spatial map is transformed into mathematical kurtosis maximization problem:

$$\mathbf{y} = (\mathbf{w}^*)^{\mathrm{T}}\mathbf{x} \tag{4}$$

where

$$\mathbf{w}^* = \underset{\mathbf{w}}{arg\,\max}\, \kappa\left(\mathbf{w}^{\mathrm{T}}\mathbf{x}\right) \tag{5}$$

and 'T' denotes the transpose operation. The well-known fast ICA algorithm [9,15] is reduced to this kurtosis maximization problem when the cubic function is selected as a choice for non-linearity.

Results

In this section, we present preliminary comparative results, in the extraction of the BCC spatial map from an RGB fluorescence image, by means of the kurtosis maximization based ICA algorithm, ratio-imaging method and optimal threshold based imaging method. For the purpose of illustration, Figs. 2 and 3 show images of the BCC tumour acquired without and with excitation with the 405 nm light sources. We base our comparative analysis mainly on how well the extracted BSS spatial maps match the visual impression of Fig. 3. To make the comparative performance analysis more fair and objective and not to rely only on the pure visual assessment, we have converted extracted spatial tumour maps into binary images. The edge detection algorithm has then been applied to binary images to calculate tumour demarcation line. Conversion of the extracted tumour maps into binary images has been done with the same threshold value for ICA and optimal threshold based image processing methods. In a case of the ratio imaging method, rather than using the contrast enhancement based post-processing, we have converted the ratio image directly into binary map, with some predefined threshold value as

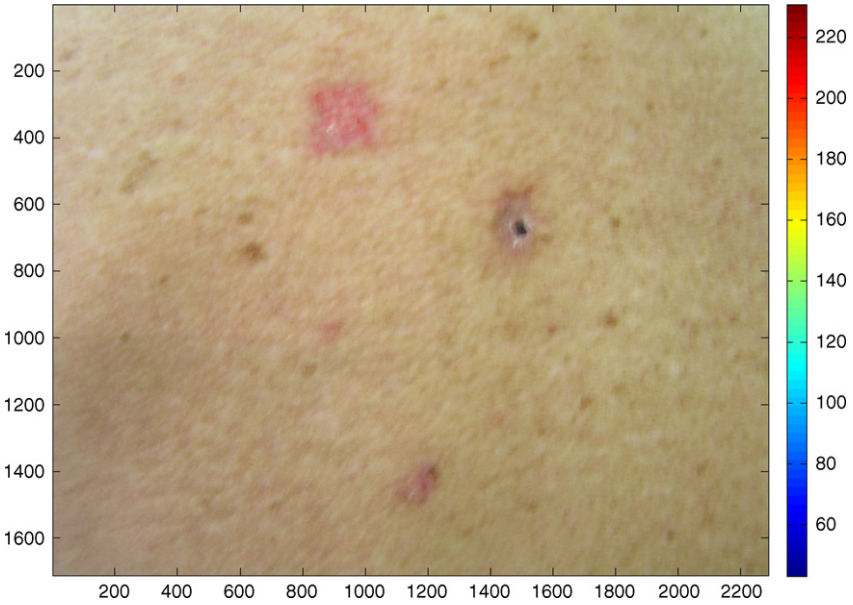

Figure 2 Natural image of the BCC without excitation by the light source.

described in the introduction. Fig. 4A shows the BCC spatial map in a false pseudo-colour obtained by the kurtosis maximization ICA algorithm, while Fig. 4B shows corresponding binary map. We have normalized intensity of the BCC spatial map to the [0, 1] interval. In that way the probability can be assigned to the extracted tumour map. The same was done for a tumour map extracted by the optimal threshold based method. Tumour demarcation line that is calculated by Canny's edge extraction algorithm from Fig. 4B, is shown in Fig. 5. Fig. 6A and B shows the binary BCC spatial maps in a false pseudo-colour obtained by the ratio-imaging algorithm, for a threshold value set to 5 and 10, respectively. These figures illustrate how the size of the spatial tumour map varies significantly with the change of the threshold value. The optimal value of the threshold is highly dependent on the intensity of the acquired fluorescence image and that is where the ratio imaging method can introduce errors in the estimation of the spatial map of the tumour. Tumour demarcation lines calculated by Canny's edge extraction algorithm, from Fig. 6A and B, are shown in Fig. 7A and B, respectively. Fig. 8A shows the BCC spatial map in a false pseudo-colour obtained by the optimal threshold based imaging method, while Fig. 8B shows corresponding binary image. Tumour demarcation line calculated by Canny's edge extraction algorithm, from Fig. 8B is shown in Fig. 9. Figs. 8 and 9 illustrate sensitivity of the optimal threshold based method on the value of the threshold coefficient taken from [4] that cannot be considered as optimal

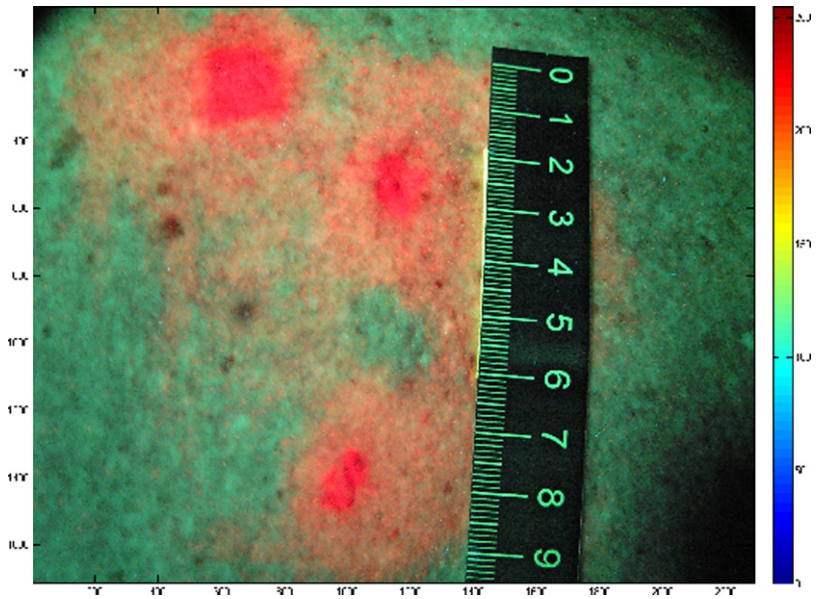

Figure 3 Image of the BCC acquired after excitation by the 405 nm light source.

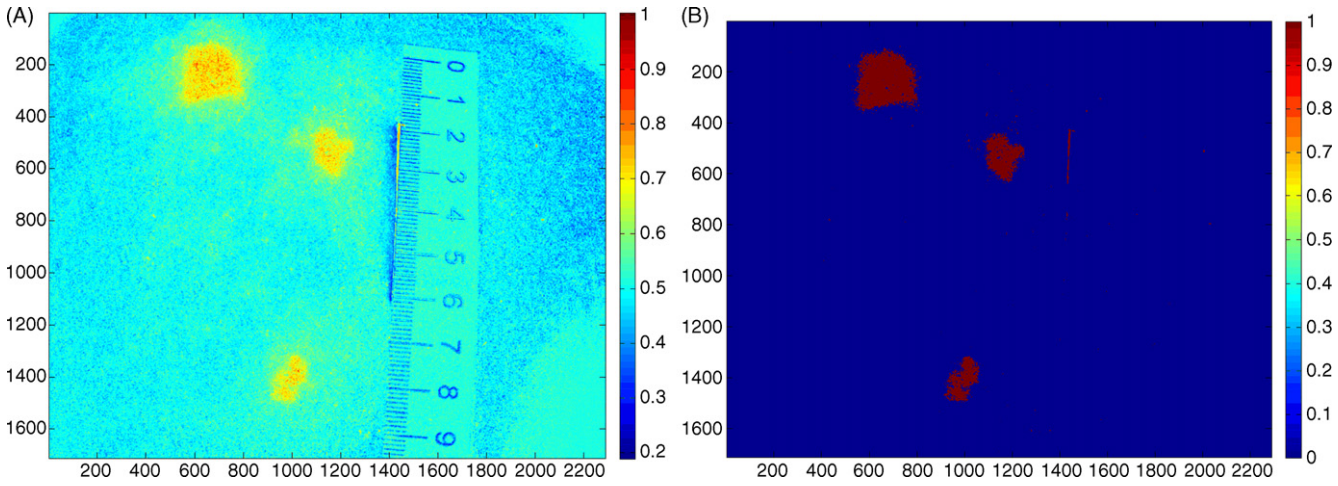

Figure 4 (A) False colored image of the BCC spatial map extracted by the kurtosis maximization ICA algorithm. (B) Binary map of the BCC spatial map extracted by the ICA algorithm.

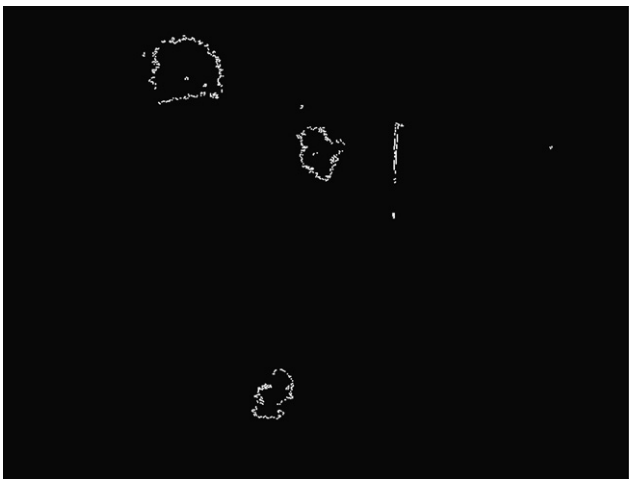

Figure 5 BCC demarcation line extracted from the binary ICA based tumor map shown in Fig. 4B.

for our image. It is very important to note that again the ICA algorithm as an unsupervised segmentation method does not depend on such arbitrarily defined threshold parameters, as it is the case with the ratio imaging and optimal threshold imaging methods. Due to this fact and due to the fact that ICA is scale invariant, it should exhibit robust performance under a variety of illuminating conditions and variation of the absolute fluorescence level. This includes illumination variation within an image resulting from skin curvature. Thus, ICA based image processing may represent a good solution for a portable optical detection system, which does not require calibration and can be operated easily.

Discussion

During the last few years, new methods for demarcation of BCC using 5-ALA PDT have been suggested [1,2,4—6,8]. A multi-spectral fluorescence imaging system for real time creation of high contrast image has been described in [8]. In particular, the ratio imaging method in combination with

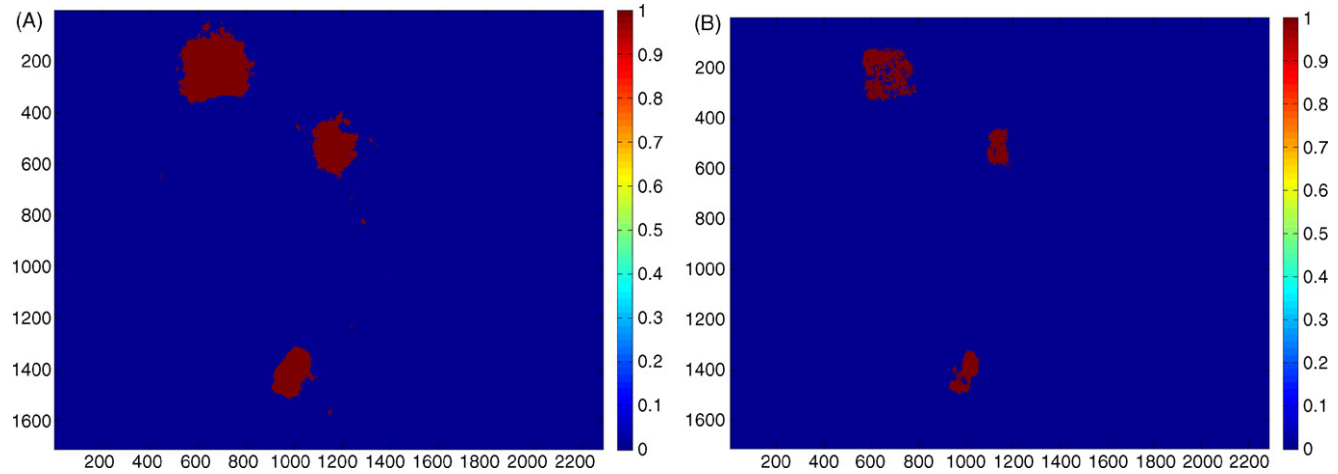

Figure 6 (A) Binary map of the BCC spatial map extracted by the ratio imaging method with a threshold value set to 5. (B) The same as part (A) except the threshold value set to 10.

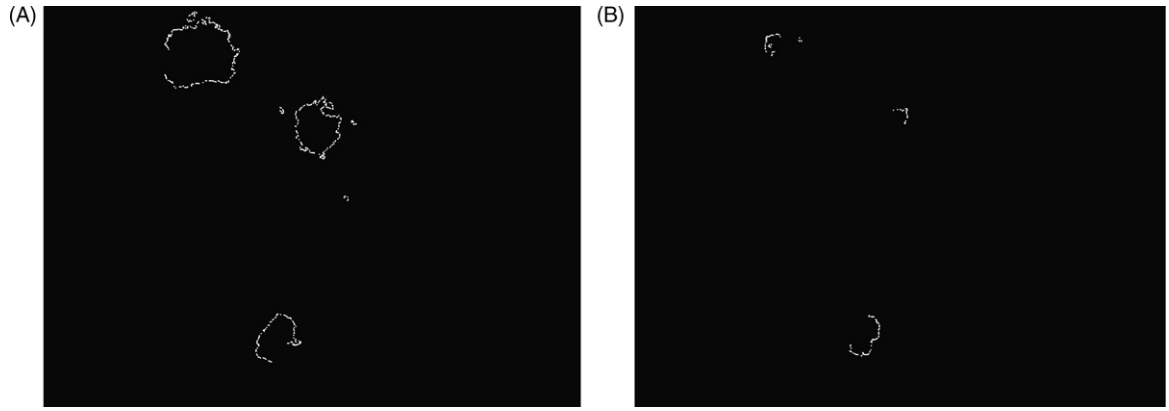

Figure 7 (A) BCC demarcation line extracted from the ratio imaging based tumour map shown in Fig. 6A. (B) BCC demarcation line extracted from the ratio imaging based tumour map with shown in Fig. 6B.

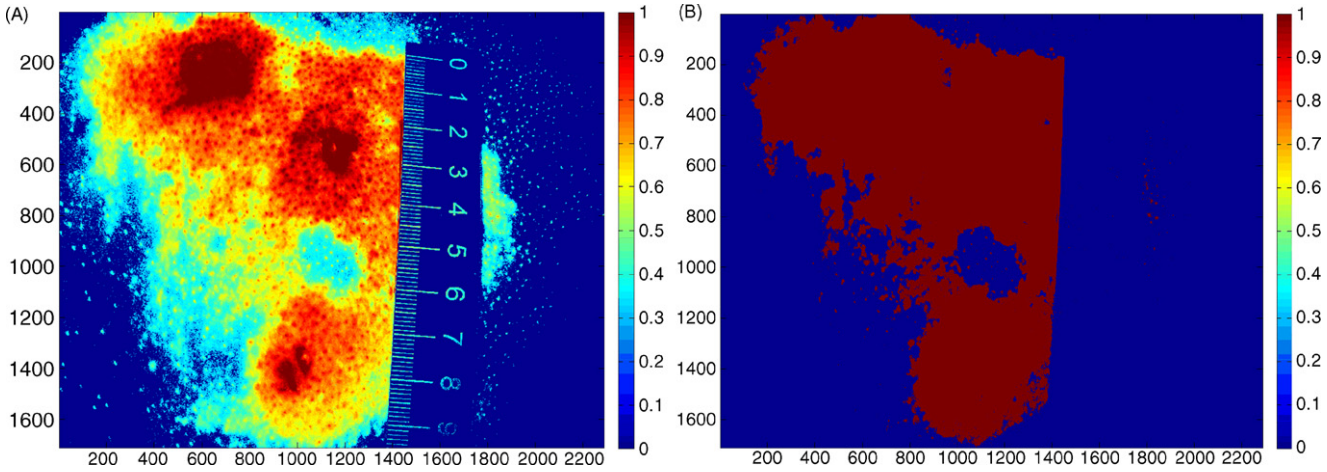

Figure 8 (A) False colored image of the BCC spatial map extracted by the optimal threshold based imaging method. (B) Binary map of the BCC spatial map extracted by the optimal threshold method.

bispectral fluorescence imaging has been proven in [1] to yield an image that is in good agreement with the actual tumour boundary found by histopathological mapping. We are aware, that the key issue when testing new diagnostic method is to correlate the derived tumour boundary with the actual extent of the tumour. Therefore, due to the lack of histological data we have compared ICA generated tumour map with the ratio imaging generated tumour map. Tumour demarcation line obtained from the ICA generated tumour map, when compared to the tumour demarcation line obtained from the ratio imaging generated tumour map, is the basis to assume that ICA may represent a useful and robust method for the indication of the tumour boundary of aggressive BCC. The robustness is with respect to the variation of the illuminating conditions and variation of the absolute fluorescence level. This stems from the scale invariance property of the ICA. Therefore, we conjecture that ICA in combination with multi-spectral imaging systems may represent a good solution for a portable optical detection system, which does not require calibration and can be operated easily. In this regard our future work will include comparative performance analysis between ICA and ratio imaging results in relation to the agreement with the histopathological mapping. We also plan in the near future to extend our analysis on more difficult cases, where intensity of the fluorescent image is rather low and important diagnostic information cannot be readily perceived by eye.

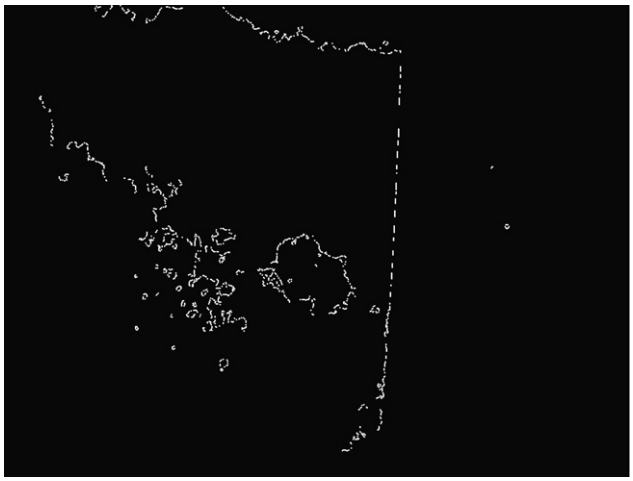

Figure 9 BCC demarcation line extracted from the binary optimal threshold imaging based tumour map shown in Fig. 8B.

Acknowledgement

The work has been supported through the projects TP-05/0098-47 and 098-0982903-2558 funded by the Ministry of Science, Education and Sport of the Republic of Croatia.

References

[1] Stenquist B, Ericsson MB, Strandeberg C, et al. Bispectral fluorescence imaging of aggressive basal cell carcinoma, combined with histopathological mapping: a preliminary study indicating a possible adjunct to Mohs micrographic surgery. Br J Dermatol 2006;154:305—9.

[2] Scott MA, Hopper C, Sahota A, et al. Fluorescence photo diagnostics and photo bleaching studies of cancerous lesions, using ratio imaging and spectroscopic techniques. Lasers Med Sci 2000;15:63—72.

[3] Bäumler W, Abels C, Szeimies RM. Fluorescence diagnosis and photodynamic therapy in dermatology. Med Laser Appl 2003;18:47—56.

[4] Ericson MB, Sandberg C, Gudmundson F, Rosén A, Larkö O, Wennberg AM. Fluorescence contrast and threshold limit: implications for photodynamic diagnosis of basal cell carcinoma. J Photochem Photobiol B: Biol 2003;69:121—7.

[5] Fischer F, Dickson EF, Pottier RH, Wieland H. An affordable, portable fluorescence imaging device for skin lesion detection using a dual wavelength approach for image contrast enhancement and aminolaevulinic acid-induced protoporphyrin IX. Part I. Design, spectral and spatial characteristics. Lasers Med Sci 2001;16:199—206.

[6] Fischer F, Dickson EFG, Pottier RH. In vivo fluorescence imaging using two excitation and/or emission wavelengths for image contrast enhancement. Vibr Spectrosc 2002;30:131—7.

[7] Koenig F, Knittel J, Stepp H. Diagnostic cancer in vivo. Science 2001;292:1401—3.

[8] Hewett J, Nadeau V, Ferguson J, et al. The application of a compact multi-spectral imaging system with integrated excitation source to *in vivo* monitoring of fluorescence during topical photodynamic therapy of superficial skin cancers. Photochem Photobiol 2001;73:278—82.

[9] Hyvärinen A, Karhunen J, Oja E. Independent component analysis. New York: Wiley Interscience; 2001.

[10] Cichocki A, Amari S. Adaptive blind signal and image processing. New York: John Wiley; 2002.

[11] Du Q, Kopriva I, Szu H. Independent component analysis for hyper spectral remote sensing. Opt Eng 2006;45:017008.

[12] Du Q, Kopriva I, Szu H. Independent component analysis for classifying multi-spectral images with dimensionality limitation. Int J Information Acquisition 2004;1:201—16.

[13] Adams JB, Smith MO, Gillespie AR. Image spectroscopy: interpretation based on spectral mixture analysis. In: Pieters CM, Englert PA, editors. Remote geochemical analysis: elemental and mineralogical composition. Cambridge, Massachusetts: Cambridge University Press; 1993. p. 145—66.

[14] Settle JJ, Drake NA. Linear mixing and estimation of ground cover proportions. Int J Remote Sensing 1993;14:1159—77.

[15] Hyvarinen A, Oja E. A fast fixed-point algorithm for independent component analysis. Neural Comput 1997;9:1483—92.